Field-aligned current distribution in the transition current system

Elena S. Belenkaya and Igor I. Alexeev
Skobeltsyn Institute of Nuclear Physics, Lomonosov Moscow State University, Vorob'evy Gory, Moscow, Russia

C. Robert Clauer Jr.
University of Michigan, Ann Arbor, Michigan, USA

Received 18 March 2004; revised 9 July 2004; accepted 30 August 2004; published 10 November 2004.

[1] The interactions of coronal mass ejections with the Earth's magnetosphere are interesting because they often lead to extreme forcing of magnetospheric convection. Here we consider the initial interaction of a CME with the magnetosphere for the specific case in which there is a sharp increase in the dynamic pressure (interplanetary shock) that is associated with a simultaneous northward turning of the interplanetary magnetic field (IMF). The magnetospheric response to such conditions has been observed to be atypical to that expected for the compression of the magnetosphere. The sudden magnetic field increase observed at low-latitude ground stations in response to such an event is asymmetric, with the largest field enhancement observed on the nightside and little or no field increase observed near local noon. We explain this response in terms of a temporary transition current system that is generated in the high-latitude magnetosphere in response to the northward turning of the IMF. In this paper we consider the dependence of the distribution of field-aligned currents in the transition current system to the radial and azimuthal components of the IMF. Model results are compared with the onground magnetometer data during 31 March 2001 storm sudden commencement (SSC). *INDEX TERMS:* 2708 Magnetospheric Physics: Current systems (2409); 2740 Magnetospheric Physics: Magnetospheric configuration and dynamics; 2784 Magnetospheric Physics: Solar wind/magnetosphere interactions; 2776 Magnetospheric Physics: Polar cap phenomena; 2736 Magnetospheric Physics: Magnetosphere/ionosphere interactions; *KEYWORDS:* magnetosphere, current systems, solar wind/magnetosphere interaction, polar cap phenomenon, magnetosphere/ionosphere interaction

Citation: Belenkaya, E. S., I. I. Alexeev, and C. R. Clauer Jr. (2004), Field-aligned current distribution in the transition current system, *J. Geophys. Res.*, *109*, A11207, doi:10.1029/2004JA010484.

1. Introduction

[2] *Clauer et al.* [2001] presented an investigation of the response of the magnetosphere to a coronal mass ejection (CME) on 24 September 1998. The super-Alfvenic CME produced a sharp increase in dynamic pressure that in turn caused a sudden compression of the magnetosphere. Simultaneous with the sharp pressure increase, the interplanetary magnetic field (IMF) turned from southward to northward. The magnetospheric response to the sharp increase in solar wind dynamic pressure and sudden compression of the magnetosphere was unexpected and very different than the typical storm sudden commencement (SSC) or sudden impulse (SI). For ~30 min following the encounter at 2345 universal time (UT) on 24 September 1998, the auroral oval became thick, while the polar cap contracted. At low latitudes the ground magnetic field perturbation shows an asymmetric increase in the axial component (parallel to the dipole axis) northward on the nightside and slightly negative at local magnetic noon [*Clauer et al.*, 2001]. Typical sudden compressions are associated with a world-wide enhancement of the northward ground magnetic field at low latitudes with a slightly larger enhancement on the dayside.

[3] The theoretical investigation of the unusual response observed on 24 September 1998 produced the concept of a three-dimensional transition current system that exists for some characteristic time in the polar regions and is caused by the rotation of the interplanetary magnetic field from slightly southward to the northward simultaneous with the passage of an interplanetary shock. We present here an analysis of the dependence of the intensity and direction of the field-aligned current in the transition current system to the radial (B_x) and azimuthal (B_y) components of the IMF change and to the high-latitude ionospheric conductivity.

2. Description of the Transition Current System Model

[4] It was shown by *Clauer et al.* [2001] that a new three-dimensional current system should form during a charac-

0148-0227/04/2004JA010484

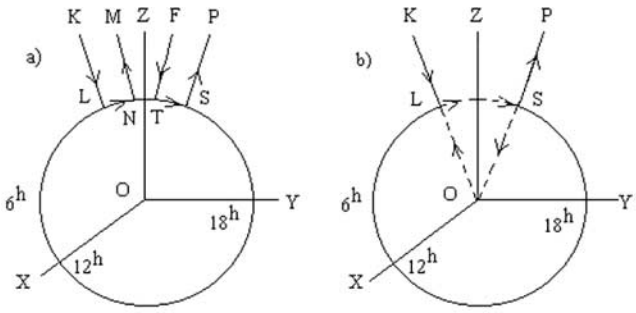

Figure 1. (a) Northern part of the transition current system. *KL* and *SP* are the Region I field-aligned currents, *LS* are their ionospheric closure currents, and *NM* and *FT* are the NBZ currents. (b) Current system connected with the Region I field-aligned currents may be represented as a sum of two current systems. The first one includes a pair of semi-infinite straight line currents *KO* and *OP*; the second one includes two straight current segments (*OL*, *SO*) and a current arc *LS* [*Belenkaya*, 2002].

teristic time period t_r after the magnetosphere encounters a CME-driven shock containing a change from southward to northward IMF. This system includes the field-aligned NBZ currents, the ionospheric Pedersen currents in the region of open field lines in the polar caps, and the field-aligned currents concentrated at the ionospheric open-closed field line boundary. This transient system was named the "transition current system." Figure 1 shows the schematic structure of this current system.

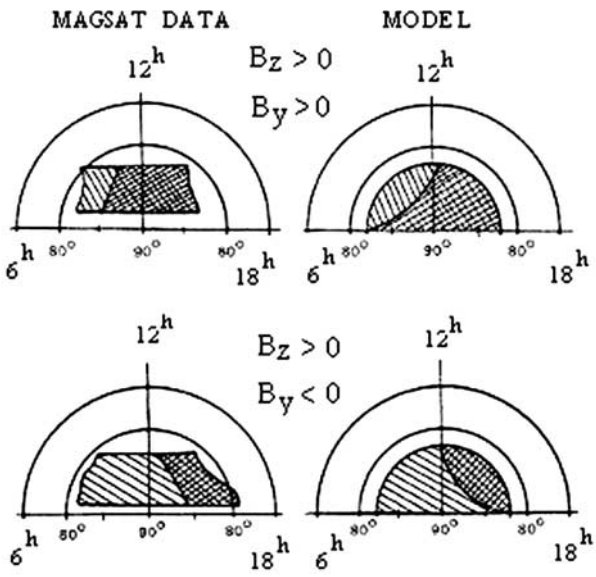

Figure 2. Dependence of the NBZ currents on the B_y IMF in the southern summer polar cap according to the MAGSAT data [*Iijima et al.*, 1984] (left) and to the calculation in the spherical model [*Alexeev and Belenkaya*, 1985] (right). Double shaded are the regions of the downward field-aligned current and shaded are the zones of the upward current.

[5] The field-aligned NBZ currents, arising during the northward IMF, are directed oppositely to the Region I field-aligned currents. They are distributed poleward of the Region I field-aligned currents and the intensity increases approaching the cusp. The relationship of the NBZ current distribution with IMF B_y in the southern polar cap during northward IMF has been obtained using magnetic field data from the MAGSAT spacecraft [*Iijima et al.*, 1984] and by the calculations using the spherical model [*Alexeev and Belenkaya*, 1985]. These correlations are shown in Figure 2 and it can be seen that the spherical magnetospheric model describes reasonably well the location of the NBZ currents in the high-latitude magnetosphere and their correlation with B_y.

[6] Figure 3 shows the high-latitude northern part of the three-dimensional transition current system associated with the northward IMF turning. The upper (bottom) panel corresponds to the case when IMF components are $B_x < 0$, $B_y = 0$, $B_z > 0$ ($B_x = 0$, $B_y < 0$, $B_z > 0$). Dashed curves mark Pedersen currents and large arrows mark Region 1 field-aligned currents. Shaded and dotted areas are for the downward and upward *NBZ* currents, respectively. In the bottom panel, the Region 1 field-aligned currents flow upward along the whole open field line boundary except the vicinity of the ionospheric cusp projection, where strong field-aligned currents of the opposite sign are concentrated.

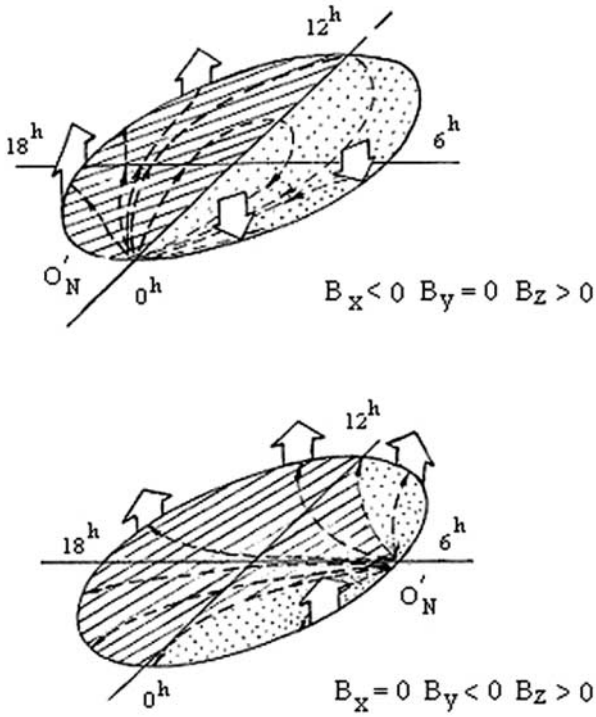

Figure 3. Field-aligned and ionospheric Pedersen (dashed curves) currents in the northern polar cap for northward IMF obtained in the spherical magnetospheric model [*Alexeev and Belenkaya*, 1985]. Thick arrows show field-aligned current concentrated at the polar cap boundary. Upward field-aligned currents distributed on the open field lines are marked by dots, and the region of downward currents is shaded.

The current strength of the Region I field-aligned currents in the transition current system can be calculated using the ionospheric electric field component normal to the open field line region boundary at the ionospheric level, $\{E_\theta\}|_{\theta_m}$:

$$I_\parallel = \Sigma_P \{E_\theta\}|_{\theta_m}. \quad (1)$$

Here Σ_P is the ionospheric height-integrated Pedersen conductivity and θ_m is the colatitude of the ionospheric open field line boundary in the northern polar cap, which is approximated by a circle with the radius $R_E \sin\theta_m$ and center O' a little bit shifted from the geomagnetic pole.

[7] *Clauer et al.* [2001] emphasized that during the characteristic time t_r after the CME-driven shock arrival, the ionospheric closure currents of the transition current system corresponded to a situation where the "effective low-latitude ionospheric conductivity" is equal to zero. Thus during this period the electric field located within the closed field line region is assumed to be equal to zero. So, the value of $\{E_\theta\}|_{\theta_m}$ is determined by the normal component of the electric field on the open field line region to its boundary.

[8] The numerical calculations of the electric field potential Φ_i in the northern polar cap were performed in the spherical model for northward IMF and were approximated by an analytical formula [*Alexeev and Belenkaya*, 1985]:

$$\Phi_i = -\frac{\delta\Phi_{npc}}{2}\left[\cot\frac{\theta_m}{2}\tan\frac{\theta}{2}\sin\varphi + \sin(2\varphi' + \varphi_m) - \sin\varphi_m\right]. \quad (2)$$

Here $\delta\Phi_{npc}$ is the potential drop across the northern polar cap. In the coordinate system (θ, φ), O' is the pole, θ is the polar angle, and φ is an azimuthal angle measured anticlockwise from the noon meridian. The other coordinate system (θ', φ') was introduced to describe the singularity in the potential and field-aligned current distributions in the open field line region of the polar cap. The pole of this coordinate system coincides with the ionospheric projection of the cusp O_N'; θ' is a polar angle, and φ' is an azimuthal angle measured anticlockwise from the direction $O_N'O'$. Potential extrema are located near the ionospheric projection of the cusp ($\theta' = 0$). Here and farther on, φ_m is an angle between the Earth-Sun line (X axis) and the IMF projection on the plane (X, Y), which is determined by equations

$$\sin\varphi_m = B_y/B_l, \quad \cos\varphi_m = B_x/B_l, \quad B_l = \sqrt{B_x^2 + B_y^2}. \quad (3)$$

[9] The first term in equation (2) is a solution of the Laplace equation for the electric potential, the second term describes a singularity character for the potential distribution for northward IMF, and the third one provides execution of the boundary conditions at the open-closed field line ionospheric boundary. From the known values of θ, φ, θ_m, and φ_m, the magnitudes of θ' and φ' can be defined by the formulas

$$\begin{aligned}\cos\theta &= \cos\theta_m\cos\theta' + \sin\theta_m\sin\theta'\cos\varphi',\\ \cos\theta' &= \cos\theta\cos\theta_m + \sin\theta\sin\theta_m\cos(\varphi_m - \varphi).\end{aligned} \quad (4)$$

From equation (2) we can determine an electric field **E** on the open field lines. **E** can be represented as a sum of two terms which are gradients (with the sign "−") of the first two terms E_1 and E_2 in the right side of equation (2). Their components normal to the open field line boundary are

$$E_{1\theta}|_{\theta_m} = \frac{|\delta\Phi_{npc}|}{2R_E}\frac{\sin\varphi}{\sin\theta_m} \quad (5)$$

and

$$E_{2\theta}|_{\theta_m} = E_{2\varphi'}\sin\varphi'|_{\theta_m}, \quad (6)$$

where

$$E_{2\varphi'}|_{\theta_m} = -\frac{|\delta\Phi_{npc}|\cos\varphi}{R_E\sin\theta'} = -\frac{|\delta\Phi_{npc}|\cos\varphi\cos\varphi'}{R_E\sin\theta_m\cos\theta_m[1-\cos(\varphi_m-\varphi)]} \quad (7)$$

(see equation (4)). From equations (6) and (7) we obtain

$$E_{2\theta}|_{\theta_m} = -\frac{|\delta\Phi_{npc}|\cos\varphi\cot\frac{\varphi_m-\varphi}{2}}{R_E\sin 2\theta_m}. \quad (8)$$

[10] The total component of the electric field on the open field lines normal to the boundary $\theta = \theta_m$ and corresponding to the northward IMF is equal to

$$E_\theta|_{\theta_m} = \frac{|\delta\Phi_{npc}|}{2R_E\sin\theta_m}\left[\sin\varphi - \frac{\cos\varphi\cot\frac{\varphi_m-\varphi}{2}}{\cos\theta_m}\right]. \quad (9)$$

From equations (1) and (9) we obtain expression for the field-aligned current at the boundary of the open field lines:

$$I_\parallel = \Sigma_P E_\theta|_{\theta_m} = \Sigma_P\frac{|\delta\Phi_{npc}|}{2R_E\sin\theta_m}\left[\sin\varphi - \frac{\cos\varphi\cot\frac{\varphi_m-\varphi}{2}}{\cos\theta_m}\right]. \quad (10)$$

[11] Taking into account that the radius of the open field line region in the polar cap is relatively small ($\cos\theta_m \sim 1$), we can obtain the approximate expression from equation (10) [*Alexeev and Belenkaya*, 1985]:

$$I_\parallel = \Sigma_P\{E_\theta\}|_{\theta_m} \approx \frac{|\delta\Phi_{npc}|}{R_E}\Sigma_P\frac{\cos\frac{\varphi+\varphi_m}{2}}{2\sin\theta_m\sin\frac{\varphi-\varphi_m}{2}}. \quad (11)$$

Here we consider the Northern Hemisphere. From the expression (10) of the field-aligned current $I_\parallel$ at the open-closed field line boundary in the northern ionosphere, the total integrated field-aligned current $J_{0\pm}$ can be obtained, J_{0+} noted currents flowing from the ionosphere and J_{0-} noted currents flowing into it.

$$J_{0\pm} = \Sigma_P|\delta\Phi_{npc}|\epsilon_\pm, \quad \epsilon = \frac{1}{2}\int\left[\sin\varphi - \frac{\cos\varphi\cot\frac{\varphi_m-\varphi}{2}}{\cos\theta_m}\right]d\varphi. \quad (12)$$

Here $\epsilon_\pm$ is the geometric factor, determining the distribution of the total upward and downward current at the ionospheric level. Integration is provided along the arcs of a circle $\theta = \theta_m$ on which the sign of $I_\parallel$ is constant; for ϵ_+ the field-aligned currents are upward (positive) and for ϵ_- the currents are downward (negative). Function $I_\parallel$ equals zero at $\varphi = \pi - \varphi_m$

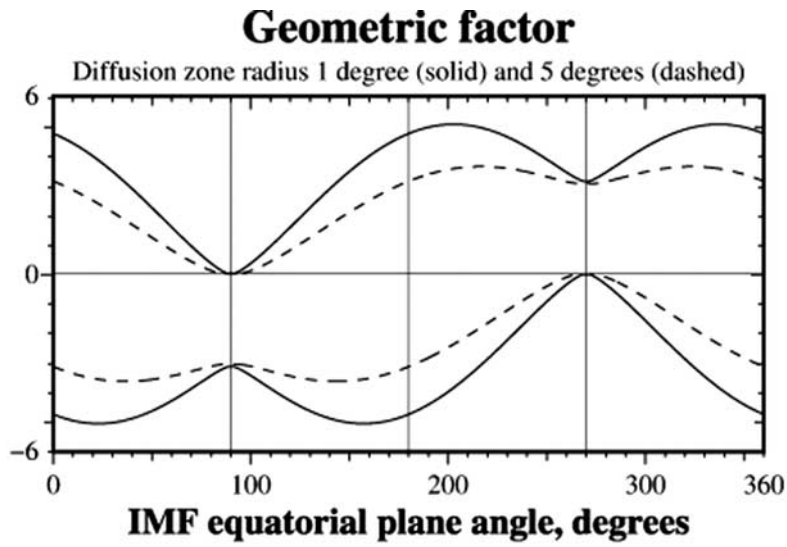

Figure 4. Geometric factor, ϵ of the Region I field-aligned current distribution in the transition current system. For two diffusion zone radius $\delta = 1°$ (solid) and $\delta = 5°$ (dashed) upper curves show ϵ_+, and bottom curves show ϵ_- dependent on the IMF equatorial plane angle, φ_m.

and approaches $\pm\infty$ at $\varphi = \varphi_m$. Thus integration of $I_\parallel$ should be done out of the vicinity of the point ($\theta = \theta_m$, $\varphi = \varphi_m$). For the scale of this vicinity the character dimension of the cusp zone can be used: $\delta \approx 1° \approx 112$ km.

[12] Intervals of integration are determined by the following inequalities:

$$\varphi_m + \delta < \varphi < \pi - \varphi_m;$$
$$0 < \varphi < \varphi_m - \delta \text{ and } \pi - \varphi_m < \varphi < 2\pi \text{ for } 0 < \varphi_m < \pi/2, \tag{13}$$

$$\pi - \varphi_m < \varphi < \varphi_m - \delta;$$
$$\varphi_m + \delta < \varphi < 2\pi \text{ and } 0 < \varphi < \pi - \varphi_m \text{ for } \pi/2 < \varphi_m < \pi, \tag{14}$$

$$\pi - \varphi_m < \varphi < 2\pi \text{ and } 0 < \varphi < \varphi_m - \delta;$$
$$\varphi_m + \delta < \varphi < \pi - \varphi_m \text{ for } \pi < \varphi_m < 3\pi/2, \tag{15}$$

$$\varphi_m + \delta < \varphi < 2\pi \text{ and } 0 < \varphi < \pi - \varphi_m;$$
$$\pi - \varphi_m < \varphi < \varphi_m - \delta \text{ for } 3\pi/2 < \varphi_m < 2\pi. \tag{16}$$

[13] Taking indefinite integral in equation (12), we obtain the following expression for ϵ: $\cos\varphi_m \ln|\sin((\varphi_m - \varphi)/2)| + ((\varphi_m - \varphi)/2)\sin_m$, in which the finite limits of integration should be inserted (see equations (13)–(16)). First terms in equations (13)–(16) correspond to ϵ_+ and the last ones correspond to ϵ_-. Geometric factor $\epsilon_\pm$ is determined by

$$\epsilon_+ = \cos\varphi_m \ln\left|\frac{\cos\varphi_m}{\sin\frac{\delta}{2}}\right| + \left(\varphi_m - \frac{\pi}{2} + \frac{\delta}{2}\right)\sin\varphi_m,$$
$$\epsilon_- = -\cos\varphi_m \ln\left|\frac{\cos\varphi_m}{\sin\frac{\delta}{2}}\right| + \left(\frac{\delta}{2} - \frac{\pi}{2} - \varphi_m\right)\sin\varphi_m \tag{17}$$
$$\text{for } 0 < \varphi_m < \pi/2,$$

$$\epsilon_+ = -\cos\varphi_m \ln\left|\frac{\cos\varphi_m}{\sin\frac{\delta}{2}}\right| - \left(\varphi_m - \frac{\pi}{2} - \frac{\delta}{2}\right)\sin\varphi_m,$$
$$\epsilon_- = \cos\varphi_m \ln\left|\frac{\cos\varphi_m}{\sin\frac{\delta}{2}}\right| + \left(\frac{\delta}{2} - \frac{3\pi}{2} + \varphi_m\right)\sin\varphi_m \tag{18}$$
$$\text{for } \pi/2 < \varphi_m < \pi,$$

$$\epsilon_+ = -\cos\varphi_m \ln\left|\frac{\cos\varphi_m}{\sin\frac{\delta}{2}}\right| + \left(\frac{\pi}{2} - \varphi_m + \frac{\delta}{2}\right)\sin\varphi_m,$$
$$\epsilon_- = \cos\varphi_m \ln\left|\frac{\cos\varphi_m}{\sin\frac{\delta}{2}}\right| + \left(\varphi_m - \frac{\delta}{2} - \frac{3\pi}{2}\right)\sin\varphi_m \tag{19}$$
$$\text{for } \pi < \varphi_m < 3\pi/2,$$

$$\epsilon_+ = \cos\varphi_m \ln\left|\frac{\cos\varphi_m}{\sin\frac{\delta}{2}}\right| + \left(\varphi_m - \frac{5\pi}{2} + \frac{\delta}{2}\right)\sin\varphi_m,$$
$$\epsilon_- = -\cos\varphi_m \ln\left|\frac{\cos\varphi_m}{\sin\frac{\delta}{2}}\right| + \left(\frac{\delta}{2} + \frac{3\pi}{2} - \varphi_m\right)\sin\varphi_m \tag{20}$$
$$\text{for } 3\pi/2 < \varphi_m < 2\pi.$$

[14] Magnitude of $\epsilon_\pm$ changes from 0 to 5 for $\delta \approx 1°$ and from 0 to 3.5 for $\delta \approx 5°$ (see Figure 4). Function ϵ_+ equals to zero at $\varphi_m = \pi/2$, when $\epsilon_- = -3$; ϵ_- equals to 0 at $\varphi_m = 3\pi/2$, when $\epsilon_+ = 3$. For $\varphi_m = 0$ or π, $\epsilon_+ = -\epsilon_- \approx 4.8$ for $\delta \approx 1°$ and $\epsilon_+ = -\epsilon_- \approx 3$ for $\delta \approx 5°$. From Figure 3 it follows that for $B_y = 0$ and $B_z > 0$ ($\varphi_m = 0$ or $\varphi_m = \pi$), both arcs of integration are equal to each other and consequently $J_{0+} = J_{0-}$. *Siscoe et al.* [2002], using a MHD simulation, found that the value of the coefficient characterizing the field-

aligned current geometry at the ionospheric level varies from 3 to 4.

3. Transition Current System at the Beginning of the 31 March 2001 Magnetic Storm

[15] The results obtained in this paper can be compared with observations of the phenomena occurring at the beginning of the 31 March 2001 storm, which was initiated by a large coronal mass ejection (CME). The CME-driven shock encountered the Earth's magnetosphere at 0051 UT on 31 March 2001. Figure 5 shows 4-min averages of the upstream IMF components from ACE shifted by the travel time from ACE to the magnetopause. This time lag is estimated to be about 40 min [*Hairston et al.*, 2003]. During approximately 6 hours before the CME arrival at Earth, the value of near-radial IMF was $\leq$5 nT and B_z was very small. Figure 5 shows that just before the encounter with CME, the IMF components were B_{x0} = 7 nT, B_{y0} = 5 nT, and $B_{z0} \approx$ 0 nT. Just behind the front of the CME (at 0010 UT on 31 March 2001) the averaged values of the IMF components were $B_{x1} = -40$ nT, B_{y1} = 12 nT, and B_{z1} = 40 nT. From equation (3) it follows that the last data correspond to $\varphi_m = 164.3°$. From Figure 4 it follows that for $\varphi_m = 164.3°$ and $\delta = 1°$ we can obtain the values $\epsilon_+ \approx 4.2$ and $\epsilon_- \approx -5$ (for $\delta = 5°$ the corresponding values are $\epsilon_+ \approx 2.6$ and $\epsilon_- \approx -3.5$). So, in the case considered here, the average value of the magnitude of ϵ is 4.6 for $\delta = 1°$.

[16] The potential drop across the polar cap can be determined using the *Hairston et al.* [2003] model. From Figure 2 of *Hairston et al.*'s [2003] paper it follows that $\delta\Phi_{npc} \approx 100$ kV at 0110 UT on 31 March 2001. *Hairston et al.* [2003] mentioned that there are no direct measurements of Σ_P during this event, so they used constant value in the typical range of 5–10 S. Following them, we used the averaged value of the integral Pedersen ionospheric conductivity Σ_P = 9 S. We chose Σ_P close to the upper limit because the precipitation electrons gave an essential contribution to high-latitude ionospheric conductivity, and at 0100 UT on 31 March 2001 the DMSP data (see http://sd-www.jhuapl.edu/Aurora/ovation/ovation_display.html) show the extreme values of the global precipitation electron energy flux (up to 126.6 MW). From equation (12) we obtain the total average field-aligned current in the transition current system $\langle J_0 \rangle = 4.2 \cdot 10^6$ A for the average value $\langle \epsilon \rangle = 4.6$.

[17] The magnetic field parallel to the dipole axes of the transition current system at the Earth's equator was found by *Clauer et al.* [2001]:

$$B_z = \mp\left(2 - \frac{1}{\sqrt{2}}\right) B_J (\sin\theta_m - \sin\delta), \qquad (21)$$

where $B_J = J_0\mu_0/2\pi R_E$. For $\langle J_0 \rangle = 4.2 \cdot 10^6$ A, B_J = 130.2 nT and $B_z = \mp 35.5$ nT (the upper sign corresponds to noon). The duration of the transition current system depends on the time of the magnetospheric convection reconstruction. This time can be calculated as a ratio of the length of the open field line bundle (208 R_E) to the solar wind velocity (570 km/s). This value is 39 min.

[18] The sharp increase in the solar wind dynamic pressure that accompanied the CME arrival caused a decrease in the subsolar point distance, R_1. Dependence of R_1 on the density n and velocity V of the solar wind was obtained by *Alexeev et al.* [2000]. If n is measured in cm^{-3} and V is measured in km/s, then R_1 in R_E is given by

$$R_1 = 100 \cdot \left(nV^2\right)^{-1/6}. \qquad (22)$$

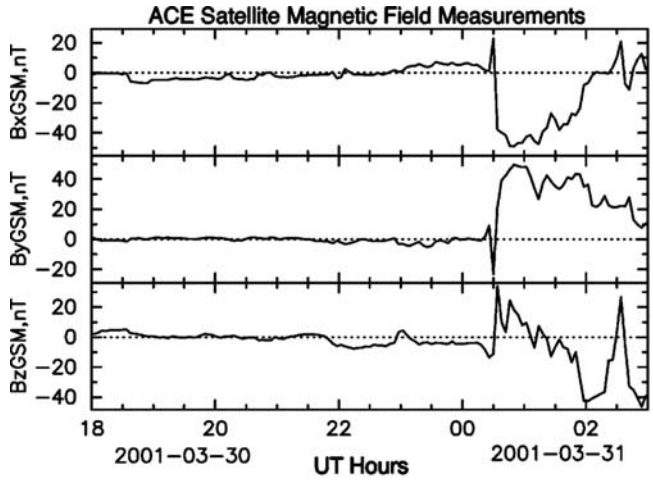

Figure 5. B_x, B_y, and B_z IMF components in GSM coordinates measured at the ACE spacecraft and time shifted by 40 min corresponding to the travel time from ACE to the magnetopause. The horizontal axis shows UT hours from 1800 UT on 30 March to 0300 UT on 31 March.

[19] The values of the upstream solar wind density n_0 and velocity V_0 (see Figure 6) were obtained from the plasma-merged 4-min ACE data set created at NSSDC as part of preparing ACE data for OMNI. Input to the NSSDC data set were 64-s SWERAM plasma data (PI: D. McComas). The time delay is taken into account. According to these data, before the CME arrival n_0 = 13 cm^{-3} and V_0 = 410 km/s, and after the CME arrival n_1 = 100 cm^{-3} and V_1 = 570 km/s. In this case, owing to the encounter with the coronal mass ejection, R_1 decreased from R_{10} = 8.77 R_E to R_{11} = 5.62 R_E. Figure 6 shows that the value of D_{st} began to grow after the IMF turned southward.

[20] The magnetic field z component caused by the magnetopause currents screening the dipole field, B_{sdz}, depends on the R_1. An approximate value at the X axes is given by *Clauer et al.* [2001]:

$$B_{sdz} = 19.5\,[\mathrm{nT}]\left(\frac{10\,R_E}{R_1}\right)^3\left(1 + \frac{x}{R_1}\right), \qquad (23)$$

where x and R_1 are measured in R_E. Owing to the compression of the dayside magnetopause (from R_{10} = 8.77 R_E to R_{11} = 5.62 R_E) B_{sdz} increased from 32.03 nT to 129.78 nT at noon ($x = 1R_E$) and from 25.4 nT to 90.18 nT at night ($x = -1R_E$). The corresponding increase in B_{sdz} was $\Delta B_{\text{sdz-noon}}$ = 97.75 nT and $\Delta B_{\text{sdz-night}}$ = 64.78 nT at noon and at night, respectively. Thus the average increase in B_{sdz}

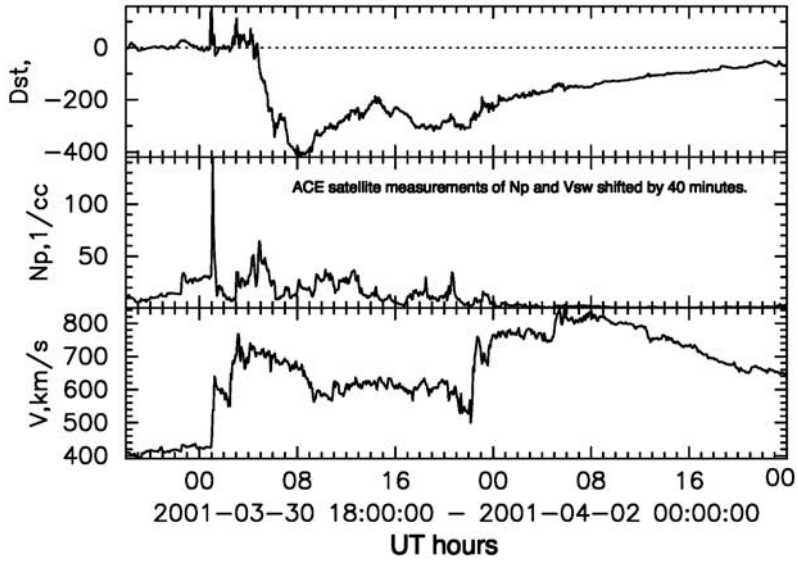

Figure 6. D_{st} at 1-min resolution computed from 19 midlatitude ground magnetic observatories, ACE measurements of ion density N_p in cm^{-3}, and the solar wind velocity V_{sw} in km/s time shifted by 40 min. The horizontal axis shows UT hours from 1800 UT on 30 March to 0000 UT on 2 April. The plasma-merged 4-min ACE data set created at NSSDC. Input to the NSSDC data set were 64-s SWERAM plasma data (PI: D. McComas).

at the Earth's equator in the meridian day-night caused by the encounter with the CME was

$$\langle \Delta B_{\mathrm{sdz}} \rangle = \frac{\Delta B_{\mathrm{sdz-noon}} + \Delta B_{\mathrm{sdz-night}}}{2} = 81.26\,[\mathrm{nT}]\,. \qquad (24)$$

[21] The tail current magnetic field dependence on the geocentric distance x (in R_E) along the Earth-Sun line is given by

$$B_{tz} = -\,14.8\,[\mathrm{nT}]\frac{2.4}{\alpha_0}\left(\frac{10\,R_E}{R_1}\right)^2\left(\frac{F_{pc}}{3.7\times 10^8\,[\mathrm{Wb}]}\right) \cdot \exp\left(-\frac{x+R_2}{R_1}\right), \qquad (25)$$

where $\alpha_0 = \sqrt{1+2R_2/R_1}$, R_2 is the geocentric distance to the earthward edge of the tail current sheet (values $\alpha_0 = 2.4$, $R_1 = 10R_E$, $F_{pc} = 3.7 \times 10^8$ Wb correspond to the quiet conditions) [*Alexeev et al.*, 2000]. R_2 did not change significantly during the passage of the CME's front (as in the work of *Clauer et al.* [2001], we supposed that for the quiet conditions $R_2 \sim 7R_E$). In response to the northward turning of the IMF from the near radial orientation, the magnetic flux in the polar cap decreased during the passage of CME. Calculations using the paraboloid model gives the value of the polar cap magnetic flux before the CME arrival as $F_{pc0} = 4 \times 10^8$ Wb. According to the DMSP satellite observations, the polar cap magnetic flux reduced to $F_{pc1} = 360$ MWb at 0100 UT on 31 March 2001 (and later, at 0300 UT to 298 MWb). Changes in the magnetic flux and R_1 lead to variation of the tail current system magnetic field measured at the Earth's equator in the day-night meridian by the passage of CME. Corresponding values of α_0 before and after the CME arrival were $\alpha_{00} = 1.61$ and $\alpha_{01} = 1.87$, respectively. Thus from equation (25) it follows that $B_{\mathrm{tz0\text{-}noon}} = -12.4$ nT, $B_{\mathrm{tz1\text{-}noon}} = -14.1$ nT, $B_{\mathrm{tz0\text{-}night}} = -15.6$ nT, $B_{\mathrm{tz1\text{-}night}} = -20.1$ nT, and consequently, $\Delta B_{\mathrm{tz\text{-}noon}} = -14.1$ nT + 12.4 $nT = -1.7$ [nT], $\Delta B_{\mathrm{tz\text{-}night}} = -20.1$ nT + 15.6 $nT = -4.5$[nT], and the average variation of the tail current magnetic field produced at the Earth's equator in the day-night meridian by the passage of CME is

$$\langle \Delta B_{\mathrm{tz}} \rangle = \frac{\Delta B_{\mathrm{tz-noon}} + \Delta B_{\mathrm{tz-night}}}{2} = -3.1\,[\mathrm{nT}] \qquad (26)$$

(for example, in the similar case on 24 September 1998 [*Clauer et al.*, 2001] the contribution of the tail current system was ~2 nT).

[22] Contrary to the case of 24 September 1998, when the prestorm D_{st} was about −50 nT, on 31 March 2001, D_{st} was ≈0 nT before SSC, then sharply increased to ≥120 nT, and after 20–30 min returned to zero. In the last case we believe that the ring current was not changed in the first hour after SSC. This is due to the fact that the 1 hour delay is needed for magnetospheric convection reconstruction and for the particle injection in the ring current region. The dayside magnetosphere (and R_1) response to the solar wind shock has a small time delay (2–5 min) which is defined by the Alfvenic time and the shock propagation time from the subsolar point to cusp.

[23] In response to the CME arrival, the initial disturbance of the magnetic field at low latitudes at the Earth in the noon-midnight meridian, $\langle \Delta B \rangle$, is determined mainly by the magnetic field perturbations caused by the magnetopause currents (equation (24)), the tail current

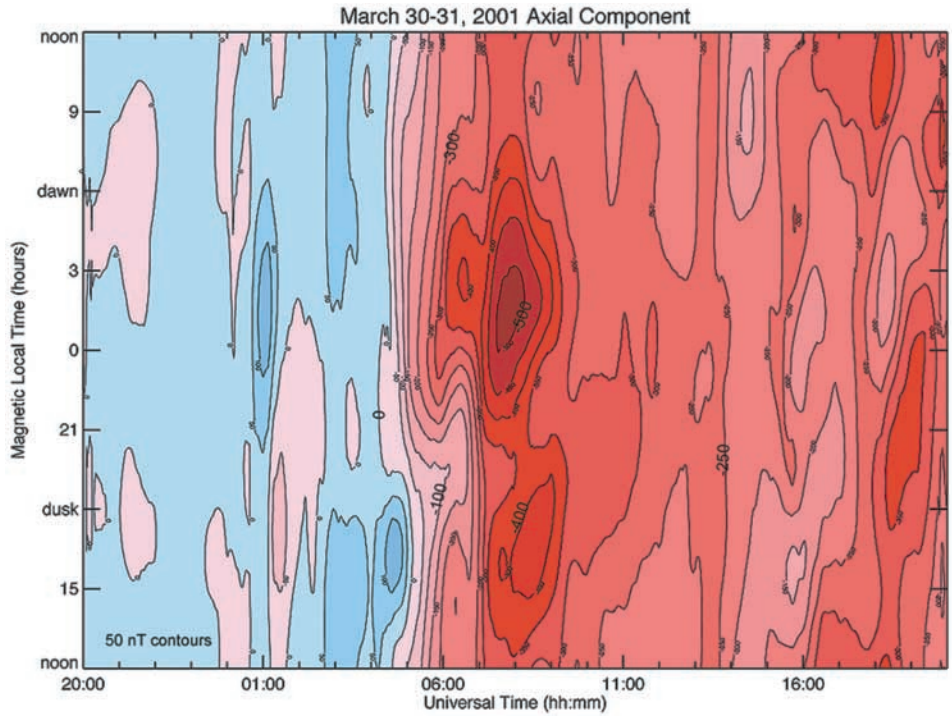

Figure 7. A LT-UT map of the axial component of the world-wide magnetic disturbance field measured by 19 low-latitude ground magnetic observatories from 2000 UT on 30 March 2001 to 2000 UT on 31 March 2001. The quiet-time field has been removed from the data using observations from the quiet day 15 March 2001. The contour step is 50 nT, with blue indicating positive disturbances and red negative disturbances [*Skoug et al.*, 2003].

system (equation (26)), and the transition current system (equation (21)):

$$\langle \Delta B \rangle = \langle \Delta B_{sdz} \rangle + \langle \Delta B_{tz} \rangle + B_z \,. \tag{27}$$

[24] Thus we obtain that at noon, the magnetic field variations at the Earth's equator should be of the order of 81.26 nT − 3.1 nT − 35.5 nT = 42.7 nT and at night 81.26 nT − 3.1 nT + 35.5 nT = 113.7 nT. These magnetic field disturbances should be observed at the Earth's equator just after the encounter with the CME carrying the northward IMF [*Clauer et al.*, 2001]. Observations described by *Skoug et al.* [2003] are consistent with our calculations. *Skoug et al.* [2003] showed a LT − UT map of world-wide magnetic disturbance field measured by 19 low-latitude ground magnetic observatories (see Figure 7 taken from *Skoug et al.* [2003]). The axial component (parallel to the dipole axis) of the disturbance field is plotted using 50 nT contours. Blue indicates positive disturbances and red indicates negative disturbances. Figure 7 shows that at 0100 UT on 31 March 2001 the observed magnetic perturbations $\langle \Delta B_{\rm obs} \rangle_{\rm noon}$ near noon were between 0 and 50 nT and at midnight they were more than 100 nT. After 15 min at noon $\langle \Delta B_{\rm obs} \rangle_{\rm noon}$ equals to zero and at midnight 100 nT > $\langle \Delta B_{\rm obs} \rangle_{\rm night}$ > 50 nT. The model predictions agree with the measurements if we take into account that the main contribution to the symmetric disturbances gives the magnetopause currents controlled by R_1. At 0115 UT on 31 March 2001 the solar wind density returned to 20 cm^{-3}. It corresponds to increasing of R_1 up to 7.4 R_E and to decrease of the magnetopause current field, $\langle \Delta B_{sdz} \rangle$, to 35.6 nT. Summarizing all terms, we receive $\langle \Delta B \rangle_{\rm night}$ = 71.1 nT and $\langle \Delta B \rangle_{\rm noon}$ = 0.1 nT. The model calculations coincide with the *Skoug et al.* [2003] results within the step of the contours in Figure 7.

4. Conclusions

[25] We have determined the distribution of the field-aligned current in the transition current system (arising in the high-latitude magnetosphere after a sudden pressure increase and simultaneous northward IMF turning) dependent on the radial and azimuthal components of the IMF. The total field-aligned currents flowing into the ionosphere and out of it at the open-closed field line boundary have been determined as a function of the polar cap potential drop, ionospheric high-integrated conductivity, and the geometric factor ϵ that describes the scheme of connection between the MHD solar wind generator and the high-latitude ionosphere. We find that ϵ can be as much as 5. This geometric factor determines the coefficient of proportionality between the value of the total field-aligned current in the transition current system and the product of the ionospheric conductivity and the polar cap potential drop. Comparison of our model calculations of the transition current system with observations of the magnetic field disturbances parallel to the dipole axis at low-latitude stations with the event on 31 March 2001 during the encounter of the dayside magnetopause with the CME carrying the northward IMF shows good agreement.

[26] **Acknowledgments.** We thank the ACE mission team and J.H. King at NSSDC and NASA's GSFC and CDAWeb for providing the the solar wind parameters. We also thank the Auroral Particles and Imagery Group at the Johns Hopkins University Applied Physics Laboratory (JHU/APL) for providing the DMSP data on the polar cap flux and the size of the polar cap oval. A portion of this research supported at the University of Michigan has been supported by the National Science Foundation Grant OPP-0220735 and NASA grant NAG5-12176. Research at Moscow State University, Moscow, Russia has been supported by the Russian Foundation of Basic Research grant 04-05-64396 and Minnayki grant NSH-2046.2003.2

[27] Arthur Richmond thanks Ruth Skoug and another reviewer for their assistance in evaluating this paper.

References

Alexeev, I. I., and E. S. Belenkaya (1985), Convection of the magnetospheric plasma on the open field line region (in Russian), *Geomagn. Aeron.*, *25*(3), 450–457.

Alexeev, I. I., E. S. Belenkaya, and C. R. Clauer Jr. (2000), A model of region 1 field-aligned currents dependent on ionospheric conductivity and solar wind parameters, *J. Geophys. Res.*, *105*(A9), 21,119–21,127.

Belenkaya, E. (2002), Influence of the interplanetary magnetic field on the formation of the magnetosphere (in Russian), *Itogy Nauki Tech. Issled. Kosmicheskogo Prostranstva VINITI*, *33a*, 235 p.

Clauer, C. R., I. I. Alexeev, E. S. Belenkaya, and J. B. Baker (2001), Special features of the September 24–27, 1998 storm during high solar wind dynamic pressure and northward interplanetary magnetic field, *J. Geophys. Res.*, *106*(A11), 25,695–25,711.

Hairston, M. R., T. W. Hill, and R. A. Heelis (2003), Observed saturation of the ionospheric polar cap potential during the 31 March 2001 storm, *Geophys. Res. Lett.*, *30*(6), 1325, doi:10.1029/2002GL015894.

Iijima, T., T. A. Potemra, and L. J. Zanetti (1984), Large-scale Birkeland currents in the dayside polar region during strongly northward IMF: A new Birkeland current system, *J. Geophys. Res.*, *89*(9), 7441–7452.

Siscoe, G. L., N. U. Crooker, and K. D. Siebert (2002), Transpolar potential saturation: Roles of region 1 current system and solar wind ram pressure, *J. Geophys. Res.*, *107*(A10), 1321, doi:10.1029/2001JA009176.

Skoug, R. M., et al. (2003), Tail-dominant storm main phase: 31 March 2001, *J. Geophys. Res.*, *108*(A6), 1259, doi:10.1029/2002JA009705.

E. S. Belenkaya and I. I. Alexeev, Institute of Nuclear Physics, Moscow State University, Moscow, 119992, Russia. (elena@dbserv.sinp.msu.ru; alexeev@dbserv.sinp.msu.su)

C. R. Clauer Jr., University of Michigan, 2455 Hayward, Ann Arbor, MI 48109-2143, USA. (rclauer@umich.edu)